

Nonlinear refraction-diffraction of water waves: The Complementary Mild-Slope Equations

Yaron Toledo and Yehuda Agnon

Civil and Environmental Engineering, Technion, Haifa, Israel.

(Received)

A second order nonlinear frequency domain model extending the linear Complementary Mild-Slope Equation (CMSE) is presented. The nonlinear model uses the same stream-function formulation as the CMSE. This allows the vertical profile assumption to accurately satisfy the kinematic bottom boundary condition in the case of nonlinear triad interactions as well as for the linear refraction-diffraction part. The result is a model with higher accuracy of wave-bottom interactions including wave-wave interaction. The model's validity is confirmed by comparison to accurate numerical models, laboratory experiments over submerged obstacles, and analytical perturbation solutions for class III Bragg resonance.

keywords: mild-slope equation, nonlinear waves, stream function formulation, Bragg resonance, coastal and offshore engineering.

1. Introduction

The irrotational flow of an incompressible homogeneous inviscid fluid is generally a three-dimensional problem. However, for practical water wave problems, this three-dimensional formulation is usually reduced to a two-dimensional one. Among the most common types of approximated equations that allow for this reduction lies the Mild-Slope (MS) type equations, which are posed in the frequency domain, and are essentially linear. In these equations, a vertical structure, which relates to the horizontal bottom case, is assumed, and the problem is averaged over the depth to enable the elimination of the vertical coordinate.

One of these MS-type equations is the Complementary Mild-Slope Equation (CMSE), which was presented by Kim & Bai (2004). Its main difference is that it is derived in terms of a stream-function vector rather than in terms of a velocity potential or the surface elevation. This enables the vertical structure to satisfy exactly the kinematic boundary condition on the uneven bottom. Whereas, in the case of the potential vertical structure assumption, which is used by other MS-type equations, the bottom boundary condition is only satisfied on a horizontal bottom.

For two-dimensional problems, the CMSE was shown to give better agreements with the exact linear theory compared to other MS-type equations (Kim & Bai (2004)). In the three-dimensional case, using the CMSE is essentially different, as it becomes a vector equation. For this problem to be well-defined, the equation needs to be reformulated and supplemented with additional boundary conditions. These difficulties were accounted for, and the superior accuracy of the CMSE model was reassured in the three-dimensional case as well (Toledo (2008)).

For solving nonlinear problems, Kaihatu & Kirby (1995) extended the work of Agnon *et al.* (1993), and constructed a model consisting of a set of MS equations coupled by quadratic nonlinear terms, which account for resonant triad interactions. Still, the potential formulation, which does not satisfy exactly the bottom boundary condition, was used in these nonlinear models. These equations were later used to study stochastic triad interaction (Agnon & Sheremet (1997), Eldeberky & Madsen (1999) and Stiassnie & Drimer (2006)).

Using *Cosserat* surfaces, Green & Naghdi (1976) developed an alternative approach for modeling incompressible fluid dynamic problems. Among other flow problems, it was as well applied to water waves (see, for example, Ertekin & Becker (1998)). Constricting this approach for sheet-like flows, Kim *et al.* (2001) have derived the Irrotational Green-Naghdi (IGN) Equations. Further more, a Lagrangian description of the IGN equations specifically for water waves was written using the stream-function formulation (Kim *et al.* (2003), Kim *et al.* (2007)).

The main objective of this work is to construct a nonlinear model using a stream-function formulation. The nonlinear model is to be consisted of a set of CMSEs coupled by quadratic nonlinear terms. This model is expected to have an improved accuracy in both the linear and the nonlinear parts due to the exact satisfaction of the kinematic boundary condition on the uneven bottom.

The paper is organized as follows: in section 2 the IGN Lagrangian is presented; a superposition of solutions with a vertical profile approximation is applied in section 3; and the nonlinear CMSE model is constructed under the assumption of time-harmonic waves in section 4. Finally, in section 5 the model's numerical results are compared

to accurate numerical simulations, laboratory experiments and analytical perturbation solutions.

2. The Irrotational Green-Naghdi Lagrangian

Define Ψ as a stream function vector

$$\Psi(\mathbf{x}, z, t) \equiv \int_{-h}^z \mathbf{u}(x, \zeta) d\zeta, \quad \mathbf{u} = (u, v), \quad \mathbf{x} = (x, y), \quad (2.1)$$

where \mathbf{u} is the horizontal velocity vector and \mathbf{x} is the horizontal position vector. From (2.1) the velocity field is defined as

$$\mathbf{u} = \frac{\partial \Psi}{\partial z}, \quad w = -\nabla \cdot \Psi. \quad (2.2)$$

The equations governing the irrotational flow of an incompressible inviscid fluid with a free surface over a horizontal bottom can be constructed using the Irrotational Green-Naghdi Equations derived from Hamilton's principle, see Kim *et al.* (2001, 2003). The Lagrangian is given by

$$\begin{aligned} \mathbf{L} &= \iint L dx dy, \\ \frac{1}{\rho} L &= \phi (\eta_t + \nabla \cdot \Psi + \Psi_z \cdot \nabla \eta)_{z=\eta} + \frac{1}{2} \int_{-h}^{\eta} (|\Psi_z|^2 + |\nabla \cdot \Psi|^2) dz - \frac{1}{2} g \eta^2. \end{aligned} \quad (2.3)$$

Here $\nabla = \left(\frac{\partial}{\partial x}, \frac{\partial}{\partial y} \right)$, $h = h(\mathbf{x})$ is the water depth, $\eta = \eta(\mathbf{x}, t)$ the surface elevation and $\phi = \phi(\mathbf{x}, t)$ is a Lagrange multiplier function. The origin is on the undisturbed water level and z is positive upward.

Taking the first variation of the Lagrangian with respect to ϕ , η and Ψ gives three Euler-Lagrange equations:

$$\frac{\delta L}{\delta \Psi} : \quad \nabla(\nabla \cdot \Psi) + \Psi_{zz} = 0 \quad -h < z < \eta \quad (2.4)$$

$$\frac{\delta L}{\delta \eta} : \quad \phi_t + \frac{1}{2} (\Psi_z)^2 + \frac{1}{2} (\nabla \cdot \Psi)^2 + g\eta = 0 \quad z = \eta \quad (2.5)$$

$$\frac{\delta L}{\delta \phi} : \quad \eta_t + \nabla \cdot \Psi + \Psi_z \cdot \nabla \eta = 0 \quad z = \eta \quad (2.6)$$

By using this formulation, Kim & Bai (2004) showed that the impermeable bottom boundary condition on $z = -h(x, y)$ is satisfied exactly, and the definition of Ψ can be used to construct a Dirichlet boundary condition,

$$\Psi = 0 \quad z = -h. \quad (2.7)$$

This together with lateral boundary conditions form a complete set of equations and boundary conditions that govern the irrotational flow of an incompressible inviscid fluid with a free surface. Equation (2.5) implies that ϕ , the Lagrange multiplier for the kinematic boundary condition on the free surface, is actually the velocity potential on the free surface, as shown by Kim *et al.* (2001).

3. The approximated Euler-Lagrange equations

Expanding equation (2.3) around $z = 0$ by use of the Taylor series up to $O((ka)^2)$ gives

$$\begin{aligned} \frac{1}{\rho}L &= \phi(\eta_t + \nabla \cdot \Psi + \Psi_z \cdot \nabla \eta + \nabla \cdot \Psi_z \eta)_{z=0} + \\ &+ \frac{1}{2} \int_{-h}^0 (|\Psi_z|^2 + (\nabla \cdot \Psi)^2) dz + \frac{1}{2} \eta (|\Psi_z|^2 + (\nabla \cdot \Psi)^2)_{z=0} - \frac{1}{2} g \eta^2 \end{aligned} \quad (3.1)$$

In order to eliminate the z -coordinate and construct a MS-type equation the vertical profile can be assumed to consist of a superposition of solutions:

$$\Psi(\mathbf{x}, z, t) = \sum_{l=1}^N f_l(k_l, h, z) \Psi_l(\mathbf{x}, t). \quad (3.2)$$

Following Kim & Bai (2004), the vertical profiles are chosen as in the linear solution of the horizontal bottom problem

$$f_l(k_l, h, z) = \frac{\sinh(k_l(h)(z+h))}{\sinh(k_l(h)h)}, \quad \omega_l^2 = g k_l \tanh(k_l h). \quad (3.3)$$

Substituting (3.2), the Lagrangian (3.1) becomes

$$\begin{aligned} \frac{1}{\rho}L &= \phi \left(\eta_t + \sum_{l=1}^N \nabla \cdot \Psi_l + \sum_{l=1}^N \bar{f}_l \Psi_l \cdot \nabla \eta + \sum_{l=1}^N (\nabla \bar{f}_l \cdot \Psi_l + \bar{f}_l \nabla \cdot \Psi_l) \eta \right) + \\ &+ IntLinPart + \frac{1}{2} \sum_{l=1}^N \sum_{m=1}^N (\bar{f}_l \bar{f}_m \Psi_l \cdot \Psi_m + (\nabla \cdot \Psi_l) (\nabla \cdot \Psi_m)) \eta - \frac{1}{2} g \eta^2 \end{aligned} \quad (3.4)$$

where

$$\bar{f}_l \equiv \frac{\partial f_l(k_l, h, z)}{\partial z} \Big|_{z=0}, \quad (3.5)$$

$$\begin{aligned} IntLinPart &\equiv \sum_{l=1}^N \sum_{m=1}^N \left(\frac{1}{2} \bar{d} \Psi_l \cdot \Psi_m + b (\nabla h \cdot \Psi_l) \nabla \cdot \Psi_m + \right. \\ &\left. \frac{1}{2} c (\nabla h \cdot \Psi_l) (\nabla h \cdot \Psi_m) + \frac{1}{2} \bar{a} (\nabla \cdot \Psi_l) (\nabla \cdot \Psi_m) \right). \end{aligned} \quad (3.6)$$

Taking the first variation of the Lagrangian (3.4) with respect to ϕ , η and Ψ_n for $n = 1, 2, \dots, N$ yield $2N + 2$ Euler-Lagrange equations:

$$\begin{aligned} \frac{\delta L}{\delta \Psi_n} &: -\nabla \phi - \nabla \phi \bar{f}_n \eta + LinPart_n + \left(\sum_{l=1}^N \bar{f}_l \Psi_l \right) \bar{f}_n \eta - \\ &- \sum_{l=1}^N (\nabla (\nabla \cdot \Psi_l) \eta + (\nabla \cdot \Psi_l) \nabla \eta) = 0 \quad (3.7) \\ \frac{\delta L}{\delta \eta} &: \phi_t + \nabla \phi \sum_{l=1}^N \bar{f}_l \Psi_l + g \eta - \end{aligned}$$

$$-\frac{1}{2} \sum_{l=1}^N \sum_{m=1}^N (\bar{f}_l \bar{f}_m \Psi_l \cdot \Psi_m + (\nabla \cdot \Psi_l)(\nabla \cdot \Psi_m)) = 0 \quad (3.8)$$

$$\frac{\delta L}{\delta \phi} : \eta_t + \sum_{l=1}^N \nabla \cdot \Psi_l + \sum_{l=1}^N \nabla \cdot (\bar{f}_l \Psi) \eta + \sum_{l=1}^N \nabla \eta \cdot (\bar{f}_l \Psi) = 0 \quad (3.9)$$

where

$$\begin{aligned} LinPart_n = & \bar{d} \Psi_n - \nabla (\bar{a} (\nabla \cdot \Psi_n) + b (\nabla h \cdot \Psi_n)) + \\ & + b (\nabla \cdot \Psi_n) \nabla h + c (\nabla h \cdot \Psi_n) \nabla h, \end{aligned}$$

and the definitions of \bar{a} , b , c and \bar{d} are

$$\begin{aligned} \bar{a}(h) &= \int_{-h}^0 f^2 dz, \quad b(h) = \int_{-h}^0 f \frac{\partial f}{\partial h} dz, \\ c(h) &= \int_{-h}^0 \left(\frac{\partial f}{\partial h} \right)^2 dz, \quad \bar{d}(h) = \int_{-h}^0 \left(\frac{\partial f}{\partial z} \right)^2 dz. \end{aligned} \quad (3.10)$$

As was shown in section 2, ϕ represents the velocity potential on the free surface, therefore

$$\nabla \phi = \Psi_z|_{z=\eta} = \sum_{l=1}^N \bar{f}_l \Psi_l + O((ka)^2). \quad (3.11)$$

Substituting (3.11) in equations (3.7), (3.8) and (3.9) yields

$$\frac{\delta L}{\delta \Psi_n} : -\nabla \phi + LinPart_n - \sum_{l=1}^N (\nabla (\nabla \cdot \Psi_l) \eta + (\nabla \cdot \Psi_l) \nabla \eta) = 0 \quad (3.12)$$

$$\frac{\delta L}{\delta \eta} : \phi_t + g\eta + \frac{1}{2} \sum_{l=1}^N \sum_{m=1}^N (\bar{f}_l \bar{f}_m \Psi_l \cdot \Psi_m - (\nabla \cdot \Psi_l)(\nabla \cdot \Psi_m)) = 0 \quad (3.13)$$

$$\frac{\delta L}{\delta \phi} : \eta_t + \sum_{l=1}^N \nabla \cdot \Psi_l + \sum_{l=1}^N \nabla \cdot (\bar{f}_l \Psi) \eta + \sum_{l=1}^N \nabla \eta \cdot (\bar{f}_l \Psi_l) = 0 \quad (3.14)$$

4. Time-harmonic wave propagation

The first step toward a formulation solely in terms of Ψ is to eliminate η from the nonlinear parts. In order to achieve that, linear relations can be applied, and η will be defined in terms of Ψ using a linearization of the kinematic boundary condition (2.6). In contrast, $\nabla \eta$ will be constructed by taking the gradient of the linear dynamic free surface boundary condition (2.5) together with (3.11). This allows for a low order of spatial derivatives of Ψ :

$$\eta = - \sum_{l=1}^N \int \nabla \cdot \Psi_l dt + O((ka)^2), \quad (4.1)$$

$$\nabla \eta = - \frac{1}{g} \sum_{l=1}^N \bar{f}_l \frac{\partial \Psi_l}{\partial t} + O((ka)^2). \quad (4.2)$$

Using the linear relations (4.1) and (4.2), equations (3.12), (3.14) and (3.13), the dependence on the surface elevation η can be factored out to yield $2N + 1$ coupled evolution equations of Ψ_n and ϕ

$$-\nabla\phi + LinPart_n + \sum_{l=1}^N \sum_{m=1}^N \left(\nabla(\nabla \cdot \Psi_l) \int \nabla \cdot \Psi_m dt + \frac{1}{g} (\nabla \cdot \Psi_l) \bar{f}_m \frac{\partial \Psi_m}{\partial t} \right) = 0 \quad (4.3)$$

$$\begin{aligned} \phi_{tt} = & g \sum_{l=1}^N \nabla \cdot \Psi_l - \sum_{l=1}^N \sum_{m=1}^N \left(g \nabla \cdot (\bar{f}_l \Psi_l) \int \nabla \cdot \Psi_m dt + \bar{f}_l \bar{f}_m \Psi_l \frac{\partial \Psi_m}{\partial t} \right) \\ & - \frac{1}{2} \sum_{l=1}^N \sum_{m=1}^N \frac{\partial}{\partial t} (\bar{f}_l \bar{f}_m \Psi_l \Psi_m - (\nabla \cdot \Psi_l) (\nabla \cdot \Psi_m)). \end{aligned} \quad (4.4)$$

The free surface elevation can be calculated afterwards using the relation

$$\eta_t + \sum_{l=1}^N \nabla \cdot \Psi_l - \sum_{l=1}^N \sum_{m=1}^N \left(\nabla \cdot (\bar{f}_l \Psi) \int \nabla \cdot \Psi_l dt + \frac{1}{g} \bar{f}_l \frac{\partial \Psi_l}{\partial t} \cdot (\bar{f}_m \Psi_m) \right) = 0 \quad (4.5)$$

In order to construct time-harmonic evolution equations, we assume Ψ_l to be of the form

$$\Psi_m(\mathbf{x}, t) = \psi_m(\mathbf{x})e^{-i\omega_m t} + \psi_m^*(\mathbf{x})e^{i\omega_m t} \quad (4.6)$$

where (*) denotes the complex conjugate. The free surface elevation η and the velocity potential at the free surface ϕ can be assumed as a superposition of time-harmonic solutions as well

$$\eta(\mathbf{x}, t) = \sum_{l=1}^N (\eta_l(\mathbf{x})e^{-i\omega_l t} + \eta_l^*(\mathbf{x})e^{i\omega_l t}), \quad (4.7)$$

$$\phi(\mathbf{x}, t) = \sum_{l=1}^N (\phi_l(\mathbf{x})e^{-i\omega_l t} + \phi_l^*(\mathbf{x})e^{i\omega_l t}). \quad (4.8)$$

Substituting equations (4.6) and (4.8) into equations (4.3) and (4.4), eliminating ϕ and taking into account only resonant triad interaction (i.e. the nonlinear terms that have the same angular frequency as of the linear part) yields a set of evolution equation for each harmonic ψ_n :

$$\begin{aligned} & -\nabla(a(\nabla \cdot \psi_n) + b(\nabla h \cdot \psi_n)) + (b\nabla \cdot \psi_n + c\nabla h \cdot \psi_n) \nabla h - k_n(h)^2 a \psi_n - \\ & - \sum_{l=1}^{n-1} \left(\frac{i}{\omega_{n-l}} \nabla(\nabla \cdot \psi_l) (\nabla \cdot \psi_{n-l}) - \frac{i\omega_{n-l}}{g} (\nabla \cdot \psi_l) \bar{f}_{n-l} \psi_{n-l} \right) - \\ & - \sum_{l=1}^{N-n} \left(\frac{i}{\omega_{n+l}} \nabla(\nabla \cdot \psi_l^*) (\nabla \cdot \psi_{n+l}) - \frac{i}{\omega_l} \nabla(\nabla \cdot \psi_{n+l}) (\nabla \cdot \psi_l^*) - \right. \\ & \left. - \frac{i\omega_{n+l}}{g} (\nabla \cdot \psi_l^*) \bar{f}_{n+l} \psi_{n+l} + \frac{i\omega_l}{g} (\nabla \cdot \psi_{n+l}) \bar{f}_l \psi_l^* \right) + \nabla \phi_n^{NL} = 0 \end{aligned} \quad (4.9)$$

$$\phi_n^{NL} = \frac{1}{\omega_n^2} \sum_{l=1}^{n-1} \left(\frac{ig}{\omega_{n-l}} \nabla \cdot (\bar{f}_l \psi_l) (\nabla \cdot \psi_{n-l}) - \right.$$

$$\begin{aligned}
 & -i \left(\omega_{n-l} + \frac{1}{2} \omega_n \right) \bar{f}_l \bar{f}_{n-l} \psi_l \psi_{n-l} + i \omega_n (\nabla \cdot \psi_l) (\nabla \cdot \psi_{n-l}) \Big) + \\
 & + \frac{1}{\omega_n^2} \sum_{l=1}^{N-n} \left(\frac{ig}{\omega_{n+l}} \nabla \cdot (\bar{f}_l \psi_l^*) (\nabla \cdot \psi_{n+l}) - i (\omega_{n+l} - \omega_l + \omega_n) \bar{f}_l \bar{f}_{n+l} \psi_l^* \psi_{n+l} - \right. \\
 & \left. - \frac{ig}{\omega_l} \nabla \cdot (\bar{f}_{n+l} \psi_{n+l}) \nabla \cdot \psi_l^* + i \omega_n (\nabla \cdot \psi_l^*) (\nabla \cdot \psi_{n+l}) \right)
 \end{aligned}$$

where,

$$a(h) = \int_{-h}^0 f^2 dz - \frac{g}{\omega^2} = \frac{\coth(kh)}{2k} \left(1 + \frac{2kh}{\sinh(2kh)} \right) = -\frac{gk^2}{\omega^4} CC_g, \quad (4.10)$$

$$b(h) = \int_{-h}^0 f \frac{\partial f}{\partial h} dz = \frac{1}{4 \sinh^2(kh)} \frac{2kh \cosh(2kh) - \sinh(2kh)}{2kh + \sinh(2kh)}, \quad (4.11)$$

$$c(h) = \int_{-h}^0 \left(\frac{\partial f}{\partial h} \right)^2 dz = \frac{k}{12 \sinh^2(kh)} \frac{-12kh + 8(kh)^3 + 3 \sinh(4kh) + 12(kh)^2 \sinh(2kh)}{(2kh + \sinh(2kh))^2}, \quad (4.12)$$

This set of N coupled vector equations ($2N$ scalar ones) extends Kim and Bai's (2004) CMSE vector equation with the nonlinear triad interaction terms. If needed, ϕ_n can be calculated afterwards using the relation

$$\phi_n = -\frac{g}{\omega_n^2} \nabla \cdot \psi_n + \phi_n^{NL}. \quad (4.13)$$

5. Numerical Results

5.1. Superharmonic class III Bragg resonance

Class III Bragg resonance refers to a nonlinear wave-wave-bottom resonant triad interaction. Its resonance conditions can be satisfied by an interaction between a single wave and an undulated bottom. For the 2D problem, the superharmonic resonance creates a transmitted wave with an angular frequency 2ω and a wavenumber $2k + k_b$. Here, k_b is the wavenumber of the bottom undulation, and ω and k are the angular frequency and the wavenumber of the incident wave, which satisfy the linear dispersion relation, $\omega^2 = gk \tanh(kh)$.

The particular case of class III Bragg resonance over an oscillatory bottom was addressed using other models as well (Agnon *et al.* (1998), Liu & Yue (1998), and Madsen *et al.* (2006)). Here, the bathymetry for this numerical simulation was taken as in Liu & Yue (1998): flat bottom with a patch of 5 sinusoidal ripples, where $k_b d = 0.025$ and $k_b h = 0.325$. The patch starts at $x = 0$ and d represents its amplitude. The solution was compared to the analytical perturbation solution and the numerical solution of Liu & Yue (1998). Note that the analytical solution is an approximation, which does not contain the bound wave, and is only accurate up to $x = O(\varepsilon^{-1})$.

Figure 1 presents the numerical results of equation (4.9) with 2 harmonics except in the case of $ka = 0.06$, which was calculated using 4 harmonics. The agreement with the analytical growth of the transmitted wave amplitude is excellent for lower values of ka (0.01, 0.02, 0.03). For $ka = 0.06$, we can see that toward the end of the patch the transmitted wave amplitude growth starts to decrease comparing to the analytical perturbation solution. This is expected as the analytical solution becomes less accurate at this distance. However, the initial growth of the amplitudes agree.

For $ka = 0.03, 0.06$ Liu & Yue (1998) solved this problem as well using a High-Order Spectral (HOS) method. It appears that the bound wave was filtered out of their results as their 2nd harmonic starts with no energy, and therefore their results contain no steep undulations as the ones of the Nonlinear CMSE. In figure 1, their graphs were shifted up in the magnitude of the Nonlinear CMSE's bound wave to allow an easier comparison of the 2nd harmonic amplitude growth. Note that in any MS-type equation the bound waves are not approximated well due to the assumption of a free wave's vertical structure. Still, it is the free wave evolution that is the most important.

The exact linearized class III condition for the above problem is $(k/k_b) = 2.031$. In the Nonlinear CMSE the condition for $ka = 0.03$ was the exact one, and for $ka = 0.06$ it was 2.06. In the HOS calculations the conditions for $ka = 0.03, 0.06$ were 2.021 and 2.025 respectively. We can see very good agreement for the free wave solution between the Nonlinear CMSE and the HOS in both cases.

Mei (1985) presented a multiple-scales perturbation solution for Class I Bragg resonance, where he showed that the resonant wave gains energy from the incident wave, and then transfers it back in a harmonic way as it continues to resonate on the sinusoidal patch. The same mechanism applies to the case of class III Bragg resonance, so the linear transfer of energy is expected to apply for the lower wave steepness (ka) calculations, because the patch of 5 bottom wave-lengths lies still within $x \leq O(\varepsilon^{-1})$. For higher ka or longer patches the analytical solution should apply only as the initial growth of the transmitted wave amplitude. Figure 2 presents the resulting transmitted wave amplitude for $ka = 0.05$, $k_b d = 0.03$ and a patch of 22 sinusoidal ripples, where we can see the transfer of energy back and forth.

5.2. Submerged one-dimensional obstacle

Beji & Battjes (1993), Dingemans (1994) and Luth *et al.* (1980) conducted wave tank experiments of monochromatic waves propagating over a trapezoidal bar using different scalings. The relatively shallow water together with the changes in bathymetry give rise to near resonant interactions, which transfer energy to higher harmonics.

The experimental set-up of Dingemans (1994) consists of a trapezoidal shoal region with an up-slope and down-slope of 1:20 and 1:10 respectively from a constant depth of $h_0 = 0.8m$ to the shallow flat bar-crest at the depth of $h_{bar} = 0.2m$ and back. The bathymetry and the monitored sections are shown in figure 3. The incident wave height was $H = 4cm$ and the period $T = 2.86sec$.

The nonlinear CMSE model (4.9) was used for the calculation taking into account 4 harmonics. The results for the numerical experiment together with the wave tank ones are given in figure 4. The numerical results for the first and second harmonics seem to excellently agree with the experimental results. The accuracy of the third and fourth harmonics is not expected to be high, because the nonlinear part of the model is accurate up to $O((ka)^2)$. Still, the high harmonics behave qualitatively well. Quantitatively, after the shoal area, the error of the third harmonic wave is between 10% to 20%, and the error of the fourth is greater.

Ohyama *et al.* (1995) conducted wave tank experiments of monochromatic waves propagating toward a trapezoidal bar as well, but in their experiment the bar had steep slopes of 1:2. The main qualitative difference of this experiment is that the steep obstacle creates a significant reflected wave. The experimental set-up consists of a trapezoidal shoal region with an up-slope and down-slope of 1:2 from a constant depth of $h_0 = 0.5m$ to the shallow flat panel at the depth of $h_{bar} = 0.15m$. The bathymetry and the monitored

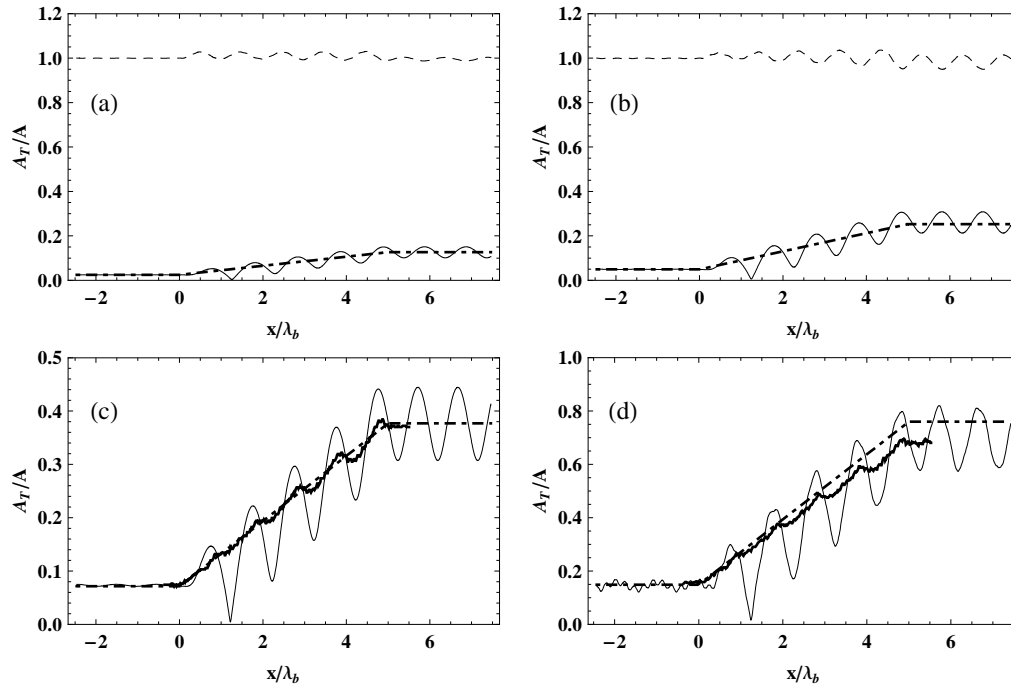


FIGURE 1. The results for class III superharmonic Bragg resonance over a patch of 5 sinusoidal ripples. The wave amplitude is normalized by the 1st harmonic incident wave amplitude and the position is normalized by the bottom wave length. Figures a, b, c and d refer to $ka = 0.01, 0.02, 0.03$ and 0.06 respectively. Dashed line represents the 1st harmonic of the Nonlinear CMSE model; Thin solid line represents the 2nd harmonic of the Nonlinear CMSE model including the bound wave; Thick solid line represents the 2nd harmonic of the High-Order Spectral method by Liu & Yue (1998); and dot-dashed line represents 2nd harmonic of the perturbation solution by Liu & Yue (1998) accurate up to $x = O(\varepsilon^{-1})$ without the bound wave.

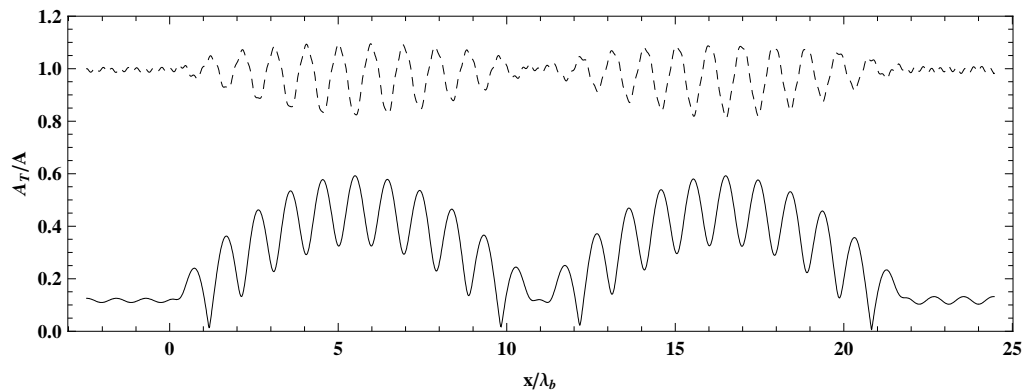


FIGURE 2. The results for the nonlinear CMSE class III Bragg superharmonic resonance over a patch of 22 sinusoidal ripples for $ka = 0.05$ and $k_b d = 0.03$. The wave amplitude is normalized by the 1st harmonic incident wave amplitude and the position is normalized by the bottom wave length. The dashed line represents the 1st harmonic of the Nonlinear CMSE model; and the thin solid line represents the 2nd harmonic of the Nonlinear CMSE model.

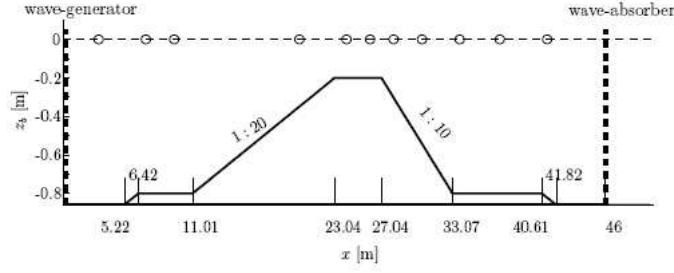


FIGURE 3. The bathymetry in the experiment of Dingemans (1994). The wavemaker is positioned at $x = 0$ with incident wave height of $H = 4\text{cm}$ and period of $T = 2.86\text{sec}$. The circles indicate the cross-sections monitored by wave gauges.

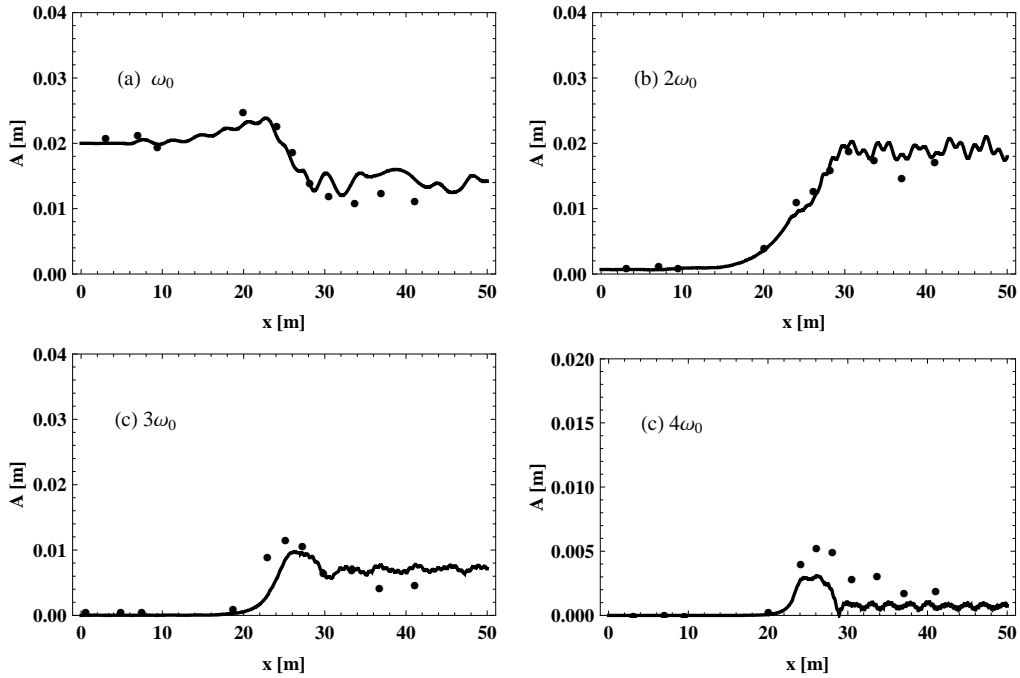


FIGURE 4. The numerical results of the nonlinear CMSE for the experiment of Dingemans (1994) (solid line) and the gauge measurements of the wave-tank experiment (solid circles). Figures a, b, c and d show the 1st, 2nd, 3rd and 4th harmonics respectively.

cross-sections are shown in figure 5. The incident wave height was $H = 5\text{cm}$ and the period $T = 2.682\text{sec}$.

The nonlinear CMSE model (4.9) was used for the calculation, again taking into account 4 harmonics. The results for the numerical experiment together with the wave tank results are shown in figure 6. The numerical results agree well with the measurements and also with accurate nonlinear numerical model runs by Ohyama & Nadaoka (1991), with the exception of some undulations in the transmitted waves. These undulations are caused by an error in modeling the bound wave. This error is inherent in MS-type models because the assumed vertical profile is for a free wave that is different in nature than the profile for a bound wave.

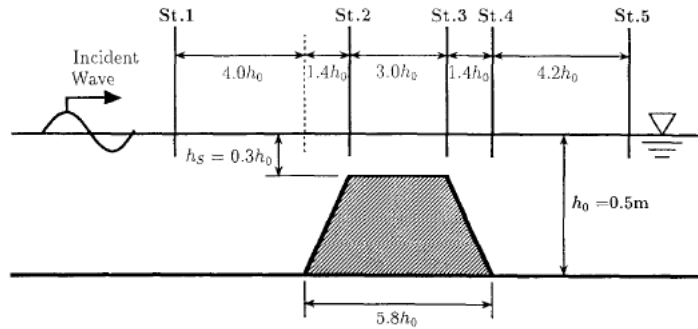


FIGURE 5. The bathymetry in the experiment of Ohya *et al.* (1995) with incident wave height of $H = 5\text{cm}$, period of $T = 2.682\text{sec}$ and constant depth of $h_0 = 0.5\text{m}$.

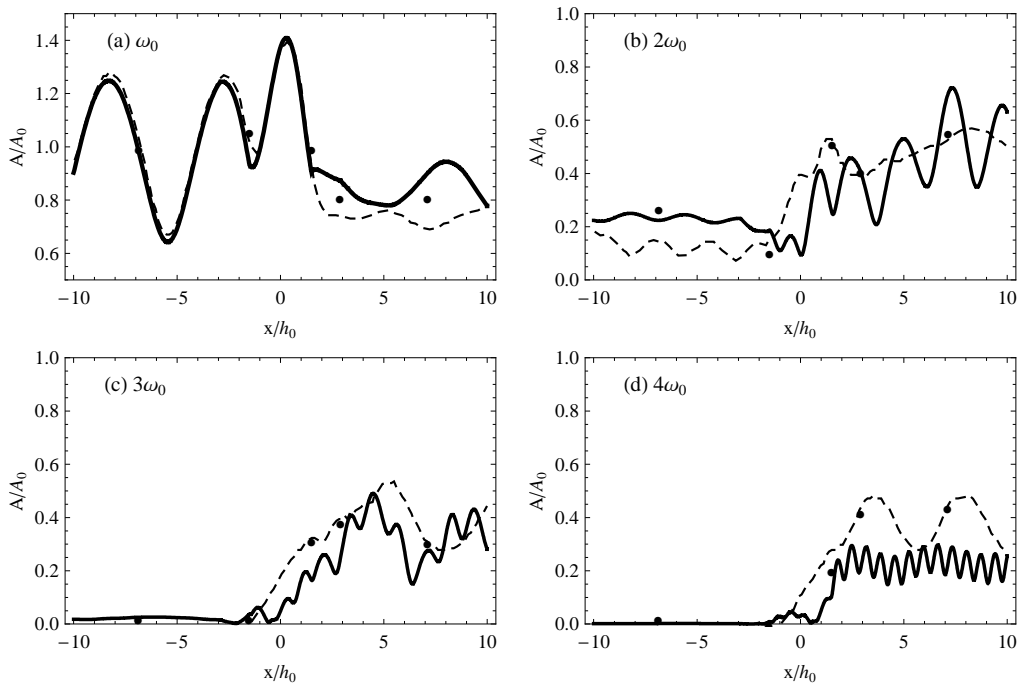


FIGURE 6. The numerical results of the nonlinear CMSE for the experiment of Ohya *et al.* (1995) shown by the solid line. The dashed lines represent the fully nonlinear solution by Ohya & Nadaoka (1991). The circles show the wave gauge measurements of the wave-tank experiment. The wave amplitude is normalized by the 1st harmonic incident wave amplitude and the position is normalized by the flat bottom depth. Figures a,b,c and d indicate the 1st, 2nd, 3rd and 4th harmonics respectively

6. Summary and conclusions

The Complementary-Mild Slope Equation was shown to give better agreement with exact linear theory compared to other MS-type equations (see Kim & Bai (2004)). The main novel concept behind it is the use of a stream-function formulation which allows the vertical profile assumption to accurately satisfy the kinematic bottom boundary condition.

In the present work, the CMSE was extended up to second order to enable nonlinear

coupling between frequency components. This was done by applying Hamilton's principle to the Irrotational Green-Naghdi Lagrangian. The nonlinear CMSE exploits the same advantages of the linear CMSE also for nonlinear triad interactions resulting in higher accuracy of the interactions between the waves and the bottom and an improved energy transfer between modes.

The model's validity is confirmed by comparison to an accurate numerical model and laboratory experiments over submerged obstacles, and to an analytical perturbation solution of class III Bragg resonance. The results give good agreements, which reassure the use of the nonlinear CMSE for practical problems.

This model is elliptic in nature and allows for solving problems that include reflection and refraction, as in harbor design. It is especially economic for narrow banded wave spectra, as the number of triad interactions is relatively small. For broad banded waves, the High-Order Boussinesq models may be more economic, even though they need to be integrated in the time domain as well.

This research was supported by the US-Israel Binational Science Foundation (Grant 2004-205) and by the Germany-Israel (BMBF-MOST) Joint Research program (Grant 1946).

REFERENCES

- AGNON, Y., PELINOVSKY, E. & SHEREMET, A. 1998 Disintegration of cnoidal waves over smooth topography. *Studies in Applied Math.* **101** (1), 49–71.
- AGNON, Y. & SHEREMET, A. 1997 Stochastic nonlinear shoaling of directional. *J. Fluid Mech.* **345**, 79–99.
- AGNON, Y., SHEREMET, A., GONSALVES, J. & STIASSNIE, M. 1993 Nonlinear evolution of a unidirectional shoaling wave field. *Coast. Eng.* **20**, 29–58.
- BEJI, S. & BATTJES, J. A. 1993 Experimental investigation of wave propagation over a bar. *Coast. Eng.* **19**, 151–162.
- DINGEMANS, M.W. 1994 Comparison of computations with Boussinesq-like models and laboratory measurements. *Tech. Rep.* h1684.12. Delft-hydraulics.
- ELDEBERKY, Y. & MADSEN, P. A. 1999 Deterministic and stochastic evolution equations for fully dispersive and weakly nonlinear waves. *Coastal Eng.* **38** (1), 1–24.
- ERTEKIN, R. C. & BECKER, J. M. 1998 Nonlinear diffraction. of waves by a submerged shelf in shallow water. *J. of Offshore Mech. and Arctic Eng.* **120** (4), 212–220.
- GREEN, A. E. & NAGHDI, P. M. 1976 Oblique wave incidence on a plane beach: the classical problem revisited. *Proc. R. Soc. London A* **347**, 447–473.
- KAIHATU, J. M. & KIRBY, J. T. 1995 Nonlinear transformation of waves in finite water depth. *phys. Fluids* **8**, 175–188.
- KIM, J. W., BAI, K.J., ERTEKIN, R. C. & WBSTER, W. C. 2001 A derivation of the Green-Naghdi equations for irrotational flows. *J. of Eng. Math.* **40**, 17–42.
- KIM, J. W. & BAI, K. J. 2004 A new complementary mild-slope equation. *J. Fluid Mech.* **511**, 25–40.
- KIM, J. W., BAI, K. J., ERTEKIN, R. C. & WBSTER, W. C. 2003 A strongly nonlinear model for water waves in water of variable depth - the irrotational Green-Naghdi model. *J. of Offshore Mech. and Arctic Eng.* **125**, 25–32.
- KIM, J. W., ERTEKIN, R. C. & BAI, K. J. 2007 Linear and non-linear wave models based on Hamilton's principle and stream-funcion theory: CMSE and IGN. *Proc. of the 26th Int. Conf. on Offshore Mech. and Arctic Eng.* **29747**, 1–8.
- LIU, Y. & YUE, D. K. P. 1998 On generalized Bragg scattering of surface waves by bottom ripples. *J. Fluid Mech.* **356**, 297–326.
- LUTH, H. R., KLOPMAN, G. & KITOU, N. 1980 Kinematics of waves breaking partially on an offshore bar; ldv measurements for waves with and without a net onshore current. *Tech. Rep.* h1573. Delft-hydraulics.

- MADSEN, P.A., FUHRMAN, D.R. & WANG, B. 2006 A Boussinesq-type method for fully nonlinear waves interacting with a rapidly varying bathymetry. *Coastal Engineering* **53**, 487–504.
- MEI, C. C. 1985 Resonant reflection of surface water waves by periodic sandbars. *J. Fluid Mech.* **152**, 315–335.
- OHYAMA, T., KIOKA, W. & TADA, A. 1995 Applicability of numerical models to nonlinear dispersive waves. *Coastal Eng.* **24**, 297–313.
- OHYAMA, T. & NADAOKA, K. 1991 Development of a numerical wave tank for analysis of nonlinear and irregular wave field. *Fluid Dyn. Res.* **8**, 231–251.
- STIASSNIE, M. & DRIMER, N. 2006 Prediction of long forcing waves for harbor agitation studies. *Journal of Waterway, Port, Coastal, and Ocean Eng.* **132** (3), 166–171.
- TOLEDO, Y. 2008 Refraction and diffraction of linear and nonlinear waves. PhD thesis, Technion - Israel Institute of Technology.